



This is a repository copy of *GnIH secreted by green light exposure, regulates bone mass through the activation of Gpr147*.

White Rose Research Online URL for this paper:

<https://eprints.whiterose.ac.uk/222352/>

Version: Published Version

Article:

You, Y. orcid.org/0000-0002-0345-6201, Huo, K., He, L. et al. (11 more authors) (2025) GnIH secreted by green light exposure, regulates bone mass through the activation of Gpr147. *Bone Research*, 13. 13. ISSN 2095-4700

<https://doi.org/10.1038/s41413-024-00389-7>

Reuse

This article is distributed under the terms of the Creative Commons Attribution (CC BY) licence. This licence allows you to distribute, remix, tweak, and build upon the work, even commercially, as long as you credit the authors for the original work. More information and the full terms of the licence here:

<https://creativecommons.org/licenses/>

Takedown

If you consider content in White Rose Research Online to be in breach of UK law, please notify us by emailing eprints@whiterose.ac.uk including the URL of the record and the reason for the withdrawal request.



eprints@whiterose.ac.uk
<https://eprints.whiterose.ac.uk/>



ARTICLE OPEN

GnIH secreted by green light exposure, regulates bone mass through the activation of Gpr147

Yu You^{1,2}, Konglin Huo^{1,2}, Liang He², Tongyue Wang², Lei Zhao², Rong Li², Xiaoqing Cheng¹, Xuebin Ma^{1,2}, Zhiying Yue³, Stefan Siwko⁴, Ning Wang^{5,6}, Lujian Liao¹, Mingyao Liu¹ and Jian Luo²

Reproductive hormones associated with the hypothalamic-pituitary-gonadal (HPG) axis are closely linked to bone homeostasis. In this study, we demonstrate that Gonadotropin inhibitory hormone (GnIH, one of the key reproductive hormones upstream of the HPG axis) plays an indispensable role in regulating bone homeostasis and maintaining bone mass. We find that deficiency of GnIH or its receptor Gpr147 leads to a significant reduction in bone mineral density (BMD) in mice primarily by enhancement of osteoclast activation in vivo and in vitro. Mechanistically, GnIH/Gpr147 inhibits osteoclastogenesis by the PI3K/AKT, MAPK, NF- κ B and Nfatc1 signaling pathways. Furthermore, GnIH treatment was able to alleviate bone loss in aging, ovariectomy (OVX) or LPS-induced mice. Moreover, the therapy using green light promotes the release of GnIH and rescues OVX-induced bone loss. In humans, serum GnIH increases and bone resorption markers decrease after green light exposure. Therefore, our study elucidates that GnIH plays an important role in maintaining bone homeostasis via modulating osteoclast differentiation and demonstrates the potential of GnIH therapy or green light therapy in preventing osteoporosis.

Bone Research (2025)13:13

; <https://doi.org/10.1038/s41413-024-00389-7>

INTRODUCTION

The homeostasis of bone mass is maintained through a dynamic balance between bone formation and bone resorption.^{1–3} Disruption of either process can result in an imbalance of bone homeostasis, ultimately leading to pathological conditions such as osteoporosis.^{4–7} Hormones associated with the HPG axis include GnIH, kisspeptin, Gonadotropin-releasing hormone (GnRH), Follicle-stimulating hormone (FSH), Luteinizing hormone (LH), estrogen, and testosterone.^{8,9} Evidence suggests that, besides estrogens and androgens, upstream reproductive hormones associated with the HPG axis also play a crucial role in regulating bone homeostasis,^{8,10,11} including FSH and LH,¹² GnRH,^{8,13} kisspeptin,^{14,15} and upstream key reproductive hormones can directly affect bone tissue. However, treatments targeting these hormones either have minimal or no direct effects on osteoblasts and osteoclast,⁸ or lead to severe side effects loss.^{16–21} Therefore, it is imperative to investigate the regulatory roles of other upstream reproductive hormones in maintaining bone homeostasis and explore their therapeutic potentials of preventing and treating orthopedic diseases.⁸

GnIH is a novel neuropeptide of hypothalamic origin,^{22–25} and it is a key upstream reproductive hormone involved in the regulation of the HPG axis and acts to inhibit reproduction.^{26–29} Accumulating evidence suggests that GnIH acts on GnRH neurons by binding G protein-coupled receptor 147 (GPR147) and regulates the function of GnRH release and synthesis.^{30–34} The use of GnRH agonists in clinical practice has shown to reduce bone mass and increase the

risk of fractures. In contrast, the use of GnRH antagonists can significantly decrease the incidence of musculoskeletal events.³⁵ These observations suggest that GnIH may play a protective role in bone. However, the molecular events underlying GnIH regulation of bone homeostasis is unclear. Intriguingly, multiple studies have revealed that green light enhances the synthesis and release of GnIH in poultry animals.^{36,37} Green light therapy has demonstrated analgesic effects in both human and murine subjects,³⁸ however, it is unknown whether green light therapy provide benefits for other diseases including osteoporosis.

In this study, we provide evidence showing that GnIH participates in regulating bone homeostasis and maintaining bone mass by suppressing the osteoclast differentiation, and that green light therapy promotes the release of GnIH and prevents bone loss by blocking osteoclast genesis in osteoporosis mouse model, as well as downregulates serum levels of bone resorption markers in human subjects. Therefore, our study suggests that green light therapy can promote GnIH release, which may provide a new strategy for preventing and treating osteoporosis.

RESULTS

GnIH/Gpr147 signaling regulates bone mass

To explore whether the novel reproductive hormone GnIH plays a role in regulating bone homeostasis, we created GnIH knockout mice (*GnIH*^{-/-} mice). We first confirmed the knockout efficiency of GnIH

¹Shanghai Key Laboratory of Regulatory Biology, Institute of Biomedical Sciences and School of Life Sciences, East China Normal University, Shanghai, PR China; ²Yangzhi Rehabilitation Hospital (Shanghai Sunshine Rehabilitation Center), Tongji University School of Medicine, Shanghai, PR China; ³Precision Research Center for Refractory Diseases, Shanghai General Hospital, Shanghai Jiaotong University, School of Medicine, Shanghai, PR China; ⁴Department of Translational Medical Sciences, Institute of Biosciences and Technology, Texas A&M University Health Science Center, Houston, TX 77030, USA; ⁵Leicester Cancer Research Centre, Department of Genetics and Genome Biology, University of Leicester, Leicester, UK and ⁶Division of Clinical Medicine, School of Medicine and Population Health, University of Sheffield, Sheffield, UK

Correspondence: Lujian Liao (ljiao@bio.ecnu.edu.cn) or Mingyao Liu (myliu@bio.ecnu.edu.cn) or Jian Luo (jluo@tongji.edu.cn)

These authors contributed equally: Yu You, Konglin Huo, Liang He

Received: 8 March 2024 Revised: 30 October 2024 Accepted: 13 November 2024

Published online: 21 January 2025

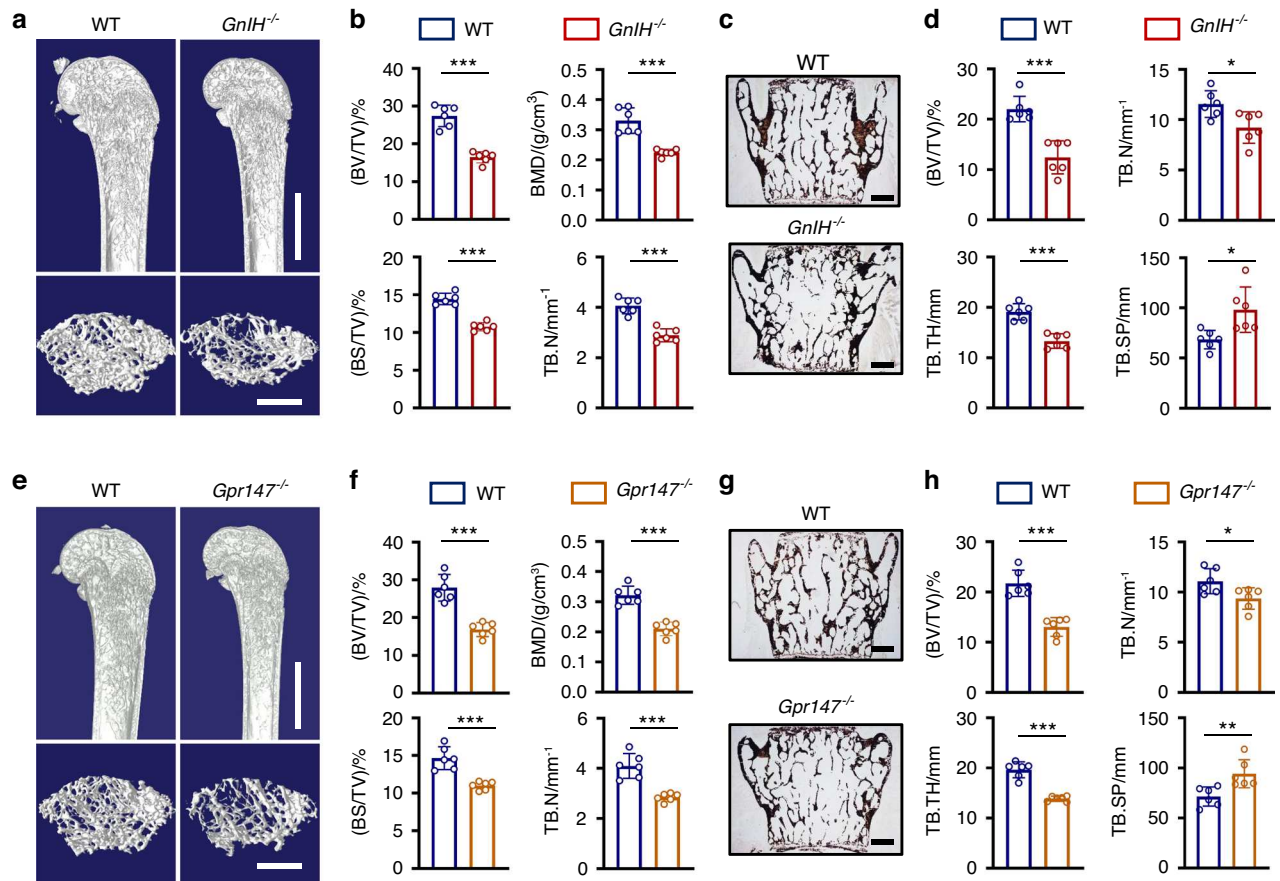


Fig. 1 Depletion of GnIH or Gpr147 decreases bone mass and leads to osteoporosis in mice. **a** Representative micro-CT images of femur (top; scale bars: 1 mm) and trabecular bone of the (bottom; scale bars: 500 μ m) from 2-month-old male WT and *GnIH*^{-/-} male mice. **b** Quantitation of femur trabecular bone parameters from WT and *GnIH*^{-/-} male mice. *n* = 6 each group. (***P* < 0.001). **c, d** The von Kossa staining images of lumbar sections from 2-month-old WT and *GnIH*^{-/-} male mice, and trabecular bone parameters were quantified. Scale bars: 500 μ m, *n* = 6 each group. (**P* < 0.05, ****P* < 0.001). **e** Representative micro-CT images of femur (top; scale bars: 1 mm) and trabecular bone (bottom; scale bars: 500 μ m) from 2-month-old male WT and *Gpr147*^{-/-} mice. **f** Quantitation of femur trabecular bone parameters from WT and *Gpr147*^{-/-} mice. *n* = 6 each group. (***P* < 0.001). **g, h** The von Kossa staining images of lumbar sections from 2-month-old WT and *Gpr147*^{-/-} male mice, and trabecular bone parameters were quantified. Scale bars: 500 μ m. *n* = 6 each group. (**P* < 0.05, ***P* < 0.01, ****P* < 0.001)

and observed that the deletion of GnIH does not affect the body weight or size of the mice (Fig. S1A, B). Then, bone mass of femurs in 2-month-old mice was measured using micro-CT. Our results revealed significant decreases of BMD, trabecular bone volume/total volume (BV/TV), external surface of the trabeculae/total sample volume (BS/TV), trabecular number (Tb.N), and trabecular thickness (Tb.Th), but an increase of trabecular separation (Tb.Sp) in *GnIH*^{-/-} compared to wild-type (WT) mice (Fig. 1a, b; Fig. S1C–E). Similar results were obtained from Von Kossa staining of lumbar vertebrae (Fig. 1c, d). To investigate whether GnIH exerts its regulatory function in osteoporosis by binding to its receptor Gpr147, we analyzed the bone density and trabecular bone parameters in femur and lumbar vertebrae from Gpr147 knockout mice (*Gpr147*^{-/-} mice). The results were similar to *GnIH*^{-/-} mice (Fig. 1e–h; Fig. S1F–J; Fig. S2A–D). Collectively, these data reveal that GnIH/Gpr147 signaling has plays a crucial role in regulating bone mass.

Deletion of GnIH or Gpr147 accelerates bone loss through enhancing osteoclast number and activity, but has little effect on osteoblast number and activity

To explore the cause of the decline in bone mass of *GnIH*^{-/-} or *Gpr147*^{-/-} mice, we first examined osteoclasts. The activity of osteoclast was significantly enhanced in femurs of *GnIH*^{-/-} mice as shown by TRAP staining and TRAP immunofluorescence staining, with the number of osteoclasts (N.Oc)/bone perimeter

(N.Oc/N.Oc/B.Pm), osteoclast surface/bone surface (Oc.S/BS) and the eroded surface/bone surface (ES/BS) all increased compared to WT mice (Fig. 2a, b; Fig. S3A, B). Similar results were found in the skulls of *GnIH*^{-/-} mice (Fig. 2c, d). Deletion of the receptor Gpr147 similarly enhanced osteoclast activity and eroded bone surface in vivo (Fig. 2e–h; Fig. S3C, D). To further examine whether GnIH directly regulated osteoclast differentiation, we evaluated the differentiation of BMMs towards osteoclasts after GnIH treatment. Remarkably, we observed a dose-dependent inhibition of osteoclast differentiation upon GnIH stimulation (Fig. 2i, j). Moreover, our research has shown that GnIH serves as a robust inhibitor of human osteoclast differentiation (Fig. 2k, l). However, GnIH exerted minimal impact on the proliferation and migration of BMMs (Fig. S4A–C). Similarly, knockout of *Gpr147* significantly promotes osteoclast differentiation and maturation (Fig. 2m, n), but has little effect on migration and proliferation of BMMs (Fig. S4D–F). Furthermore, *Gpr147*^{-/-} osteoclasts express high levels of osteoclastogenic gene transcripts when compared with control osteoclast (Fig. S4G). Moreover, osteoclasts lacking Gpr147 were no longer able to inhibit osteoclast differentiation by GnIH (Fig. S4H, I). Together, all these results confirm that knocking out *GnIH* can enhance osteoclast number, differentiation and activity through Gpr147.

We next explored whether knocking out of GnIH or Gpr147 affected bone formation and osteoblast. Our data showed that the

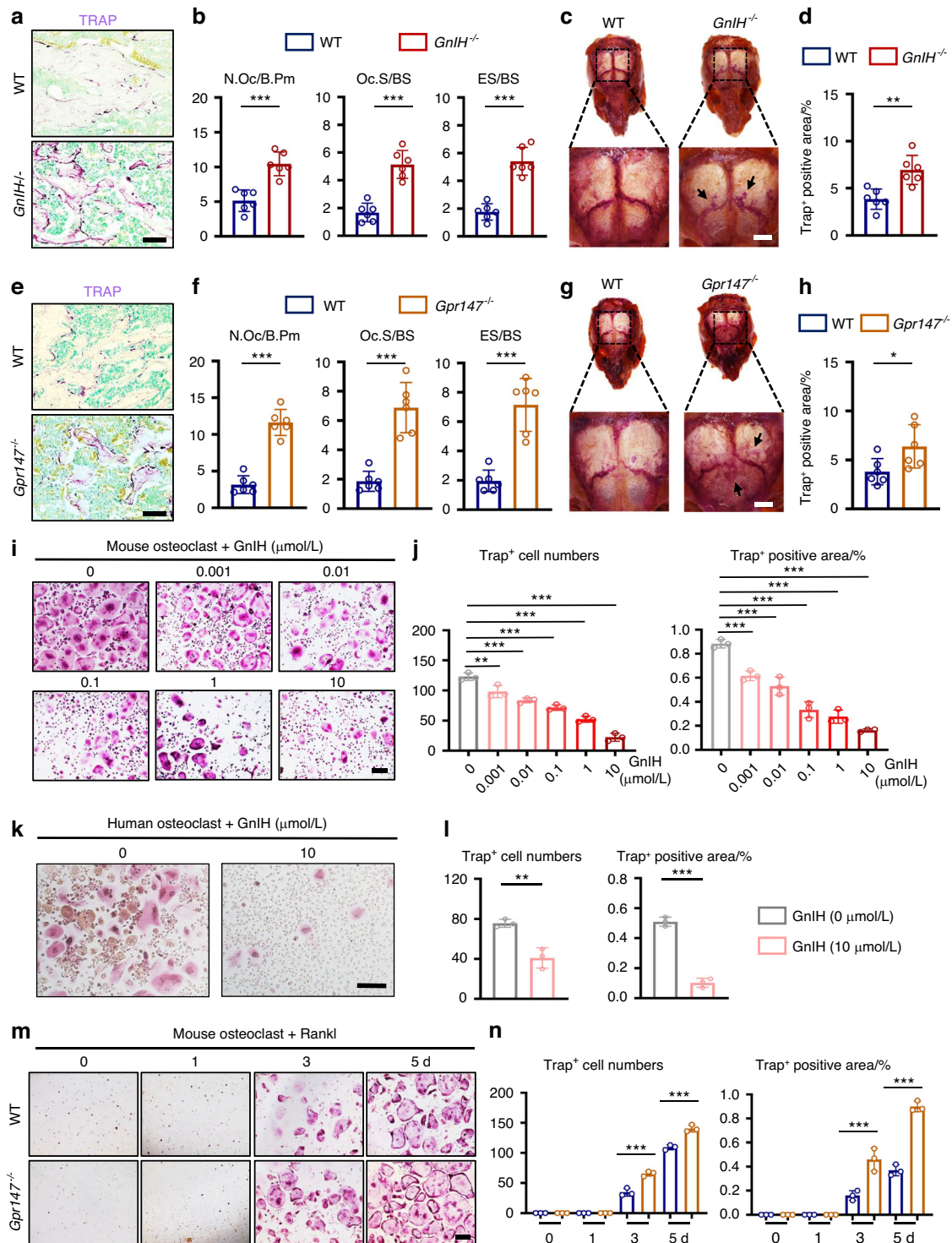


Fig. 2 GnIH and Gpr147 negatively regulates osteoclast activity. **a, b** Representative TRAP staining images from *GnIH*^{-/-} male mice. Scale bars: 100 μm. The number of N.Oc/B.Pm, Oc.S/BS and ES/BS were quantified. *n* = 6 each group. (***P* < 0.01). **c, d** Representative TRAP staining images in skulls from *GnIH*^{-/-} male mice, Scale bars: 2 mm. Trap positive area in each skull was measured and compared. *n* = 6 each group. (***P* < 0.01). **e, f** Representative TRAP staining images from *Gpr147*^{-/-} male mice. Scale bars: 100 μm. The number of N.Oc/B.Pm, Oc.S/BS and ES/BS were quantified. *n* = 6 each group. (***P* < 0.01). **g, h** Representative TRAP staining images in skull from *Gpr147*^{-/-} male mice, Scale bars: 2 mm. Trap positive area in skull were measured and compared. *n* = 6 each group. (**P* < 0.05). **i, j** Representative TRAP staining images of the differentiation of BMMs into osteoclasts in the presence of different doses of GnIH for 6 days. Trap⁺ cell numbers and Trap positive area were measured. *n* = 3 each group. Scale bars: 200 μm. (***P* < 0.01, ****P* < 0.001). **k, l** Representative TRAP staining images of the differentiation of human PBMCs into osteoclasts for 7 days. Trap⁺ cell numbers and Trap positive area were measured. *n* = 3 each group. Scale bars: 200 μm. (***P* < 0.01, ****P* < 0.001). **m, n** Representative TRAP staining images of the differentiation of *Gpr147*^{-/-} BMMs into osteoclasts for indicated times. Trap⁺ cell numbers and Trap positive area were measured. *n* = 3 each group. Scale bars: 200 μm. (***P* < 0.01, ****P* < 0.001)

bone formation rate (BFR/BS), the Mineral Apposition Rate (MAR), the number of osteoblasts (N.Ob)/bone perimeter (N.Ob/B.Pm), surface area of osteoblasts/bone surface (Ob.S/BS) and the osteoid surface/bone surface (OS/BS) all have little effect on bone formation and osteoblast in lumbar vertebrae by calcein double labeling assay and Goldner's staining in *GnlH* and *Gpr147* knockout mice (Fig. S5A–H).

All these results substantiate that the osteoporosis resulting from the knockout of *GnlH* and *Gpr147* is primarily attributed to the activation of osteoclasts and promotion of bone resorption.

GnlH derived from bone tissue can regulate osteoclastogenesis. Our data reveals a high expression of *GnlH* in bone tissue (Fig. S6A). To investigate which type of bone cells *GnlH* originates from, we randomly selected BMM as a control group, our RT-qPCR analysis in all bone cells showed that *GnlH* has strong expression in osteoclast and osteoblast, while it has limited expression in BMM, BMSC and chondrocyte (Fig. 3a). To examine whether the bone-tissue-derived *GnlH* regulates osteoclast differentiation, we analyzed osteoclastic differentiation using WT and *GnlH*^{-/-} BMM. Our results showed that knockout of *GnlH*^{-/-} largely enhanced osteoclastic differentiation and formation (Fig. 3b, c), as demonstrated by the differentiation markers *Trap*, *Ctsk*, *Nfatc1* (Fig. 3d). However, here was no difference between WT and *GnlH*^{-/-} BMMs in the level of cell proliferation and migration (Fig. S6B–D), suggesting that, besides hypothalamus, osteoclast derived *GnlH* could regulate osteoclast differentiation.

To further evaluate the function of *GnlH* in osteoclasts, taking consideration of age and age-induced bone phenotype, we analyzed the *GnlH* expression of osteoclasts derived from WT mice at different ages (2 months and 18 months) and its correlation with BMD of these mice. Our results showed that expression of *GnlH* in mouse osteoclasts is positively correlated with BMD ($P = 0.002$, $R^2 = 0.773$, $n = 12$) (Fig. 3e). We also observed that *GnlH* expression level were inversely correlated with osteoclast differentiation and TRAP expression level (Fig. 3f, g). We further examined whether the osteoblast-derived *GnlH* have regulatory effect on osteoclastogenesis by osteoblast-osteoclast co-culture experiment. Strikingly, the results showed that loss of *GnlH* in osteoblasts promoted osteoclast differentiation (Fig. 3h, i).

In addition, we found that the relative expression of Rankl at the mRNA level was increased, while the OPG expression was decreased, resulting in an enhanced ratio of Rankl to OPG in *GnlH*^{-/-} and *Gpr147*^{-/-} osteoblasts (Fig. S6E, F). To investigate whether the loss of *Gpr147* in osteoblasts has an effect on osteoclast differentiation, we further performed a *Gpr147*^{-/-} osteoblast - WT osteoclast co-culture experiment. The results showed that knockout of *Gpr147* in osteoblasts promoted the differentiation of BMMs into osteoclasts (Fig. S6G, H). Together, these results indicate that osteoblast or osteoclast secreted *GnlH* to affect osteoclast formation.

GnlH/Gpr147 regulates osteoclast differentiation through the PI3K/AKT, MAPK, NF- κ B and *Nfatc1* signaling pathways

To investigate how *GnlH/Gpr147* affects osteoclastogenesis, we performed RNA sequencing analysis on osteoclast precursors (BMM cells after two-day differentiation) from *Gpr147*-deficient and WT mice. Not surprisingly, the pathway associated with osteoclast differentiation was enriched and ranked first in *Gpr147*-deficient osteoclast precursors (Fig. 4a). Moreover, KEGG analysis revealed that deletion of *Gpr147* led to significant alterations in the phosphatidylinositol 3-kinase (PI3K)-AKT pathway in osteoclast precursor cell (Fig. 4b). To validate that *GnlH* induced osteoclast differentiation via PI3K-AKT signaling, we examined the phosphorylation levels of PI3K and AKT at various time points (0, 0.5, and 1 h) in *GnlH*-stimulated osteoclast precursors. We found that phosphorylation of PI3K and AKT were inhibited in a time-dependent manner after *GnlH* stimulation (Fig. 4c, d). Furthermore, we employed the inhibitors of PI3K/AKT signaling during

osteoclast differentiation. Our data showed that *Gpr147* knockout dramatically induced osteoclast differentiation, while the two inhibitors of the PI3K/AKT signaling pathway (Omipalisib and 3-MA) significantly suppressed *Gpr147* knockout-induced osteoclast differentiation (Fig. 4e, f; Fig. S7A, B). Because *Nfatc1* nuclear translocation is the downstream events of PI3K/AKT signaling during osteoclast differentiation,^{39–42} we next examined whether *GnlH* or the PI3K/AKT signaling inhibitors have regulatory effects on *Nfatc1* nuclear translocation. The results showed that *GnlH* significantly suppressed the nuclear translocation of *Nfatc1* (Fig. S7C, D), whilst the two PI3K/AKT signaling inhibitors can reduce *Nfatc1* nuclear translocation after knockout of *Gpr147* (Fig. 4g; Fig. S7E–G). Together, our result indicated that *GnlH/Gpr147* regulates osteoclast function through the PI3K/AKT signaling.

There is abundant evidence supporting that MAPK, NF- κ B and *Nfatc1* signaling pathways are crucial in regulating osteoclast differentiation. To investigate whether *Gpr147* also regulates osteoclast differentiation via MAPK, NF- κ B and *Nfatc1* signaling pathways, we conducted additional analyses. A time-dependent inhibition of phosphorylation on critical proteins such as p65, I κ B, p38, JNK, and ERK follows *GnlH* stimulation, coinciding with a decreased expression of *Nfatc1* (Fig. 4h, i). Thus, our data provides compelling evidence showing that *GnlH/Gpr147* regulates osteoclast function through the PI3K/AKT, MAPK, NF- κ B and *Nfatc1* signaling pathways.

GnlH inhibits bone loss induced by aging, OVX and LPS

To further validate whether *GnlH* has therapeutic effect on osteoporosis, we utilized three distinct mouse models to mimic aging-, postmenopause-, inflammation- induced osteoporosis to validate this function. First, we treated aging mouse with *GnlH* (0.1 mg/kg/day). *GnlH* treatment resulted in increased bone mass and BMD in 18-month-old mice (Fig. 5a, b, Fig. S8A), as well as in significantly inhibited osteoclast number and activity (Fig. 5c, d). Importantly, *GnlH* treatment had no evidence of toxicity or adverse effects in heart, liver, spleen, lung, and kidney tissues compared to the control group (Fig. S8B). It has been shown that IL-1 β is upregulated in the production of chronic inflammatory factors during aging.⁴³ Therefore, we evaluated whether *GnlH* affects IL-1 β -induced osteoclast differentiation and formation in vitro. *GnlH* treatment suppressed osteoclast activity in an IL-1 β inflammatory environment (Fig. S8C, D).

Next, we evaluated *GnlH* effect in OVX osteoporosis mouse model. After one month of daily intraperitoneal injection of *GnlH*, osteoclast activity was remarkably inhibited and bone loss was rescued in OVX mice (Fig. 5e–h; Fig. S8E, F). Surprisingly, the value of BMD and BV/TV in *GnlH* treatment group were almost close to the Sham operation group, suggesting that the *GnlH* could exert strong therapeutic effect on osteoporosis.

Last, using the LPS induced inflammatory bone loss mouse model, we evaluated the effect of *GnlH* on LPS-induced bone loss. Consistently, bone mass significantly increased while osteoclasts were inhibited after *GnlH* treatment (Fig. 5i–l; Fig. S9A–C). Furthermore, *GnlH* treatment suppressed LPS-induced osteoclast differentiation *ex vitro* (Fig. S9D, E), and the serum inflammatory factor TNF- α and IL-1 β were mildly decreased, whereas the level of IL-6 remains unchanged (Fig. S9F). These results suggested that in LPS-induced mice, *GnlH* treatment both affects inflammatory factor levels and slightly improves the inflammatory milieu, while also strongly inhibiting osteoclast activity. This dual action contributes to the preservation of bone mass and halting bone loss.

Taken together, these findings provide compelling evidence that *GnlH* treatment effectively enhances bone mass and inhibited osteoclast activity in aging, OVX, and LPS-induced bone loss models.

Green light promotes *GnlH* release and alleviates bone loss in OVX-induced osteoporosis mice
Green light can promote *GnlH* expression and synthesis in hypothalamus in poultry animals,^{36,37} and green light therapy has

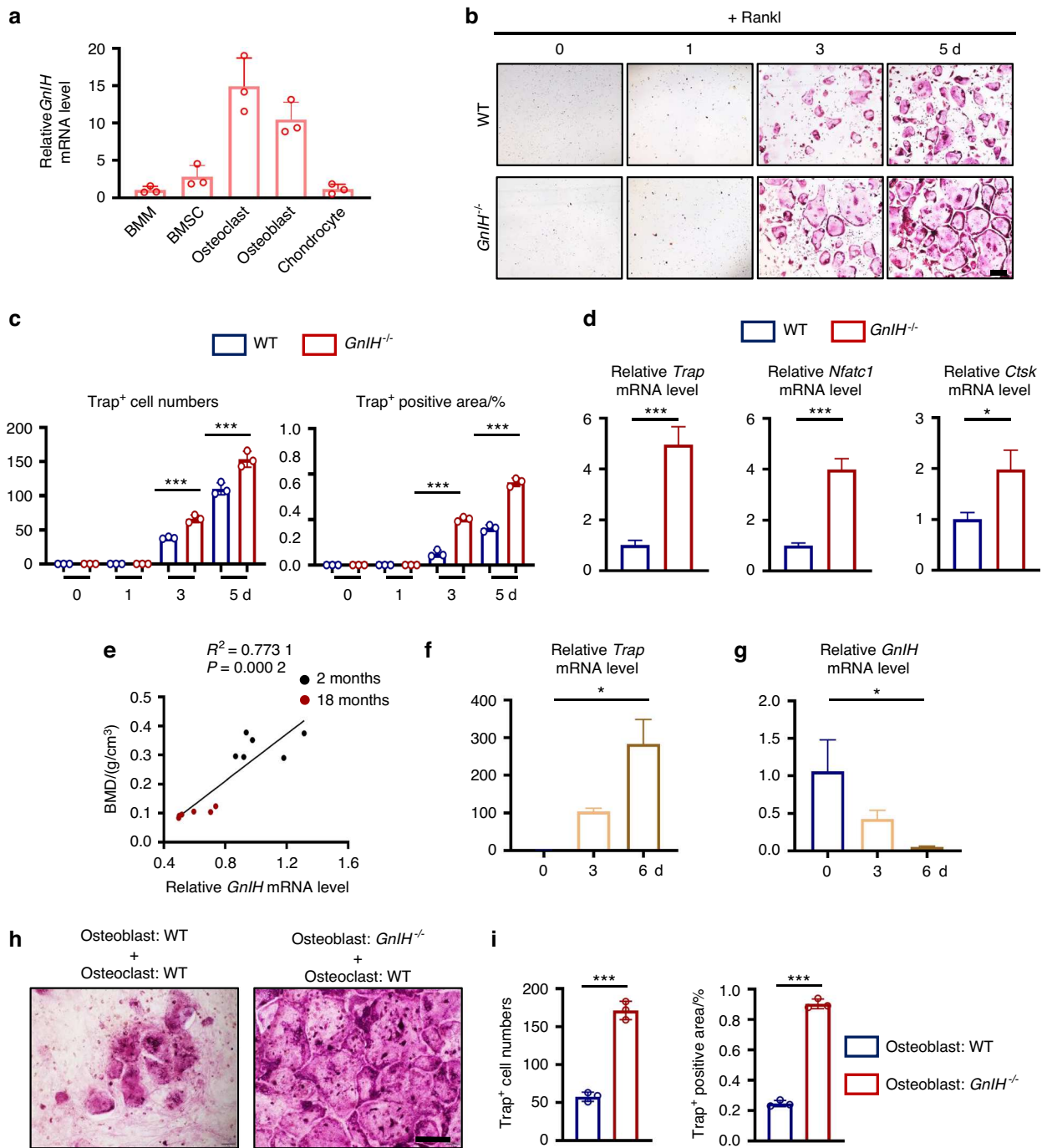


Fig. 3 GnIH derived from osteoclasts and osteoblasts negatively regulates osteoclasts activity. **a** RT-qPCR analysis of the expression of *GnIH* in cells of different bone tissues. $n = 3$ each group. **b, c** Representative TRAP staining images of the differentiation of *GnIH*^{-/-} BMMs into osteoclasts for indicated times. Trap⁺ cell numbers and area were measured. $n = 3$ each group. Scale bars: 200 μm . (** $P < 0.001$). **d** RT-qPCR analysis of the expression of *Trap*, *Nfatc1* and *Ctsk* in *GnIH*^{-/-} and WT osteoclasts. $n = 3$ each group. (* $P < 0.05$, *** $P < 0.001$). **e** Correlation between BMD of mice at different ages and the transcriptional expression of *GnIH* by osteoclasts collected at different ages (2 months or 18 months). The data were analyzed using a Pearson's correlation coefficient assay ($n = 12$). **f, g** RT-qPCR analysis of the expression of *Trap* and *GnIH* in osteoclasts at indicated times. $n = 3$ each group. (* $P < 0.05$). **h, i** Representative TRAP staining images of the differentiation of BMMs into osteoclasts cultured with WT or *GnIH*^{-/-} osteoblasts. $n = 3$ each group. Scale bars: 200 μm . Trap⁺ cell numbers and area were measured. (** $P < 0.001$)

demonstrated analgesic effects in both human and mice.³⁸ Therefore, we hypothesized that green light exposure can promote GnIH release and prevent bone loss. To verify the therapeutic effect of green light, we exposed OVX mice to green light for 8 h (8:00 am–16:00 pm) per day for 60 days (Fig. 6a). We evaluated the hypothalamic GnIH transcription level in mice, and the results

showed that exposure to green light promoted the transcriptional expression of hypothalamic *GnIH* (Fig. 6b). Consequently, serum GnIH levels were also increased after green light exposure (Fig. 6b). Furthermore, bone mass were significant increased and osteoclast number and activity were decreased in OVX mice when exposed to green light compared to OVX control group (Fig. 6c–f; Fig. S10A).

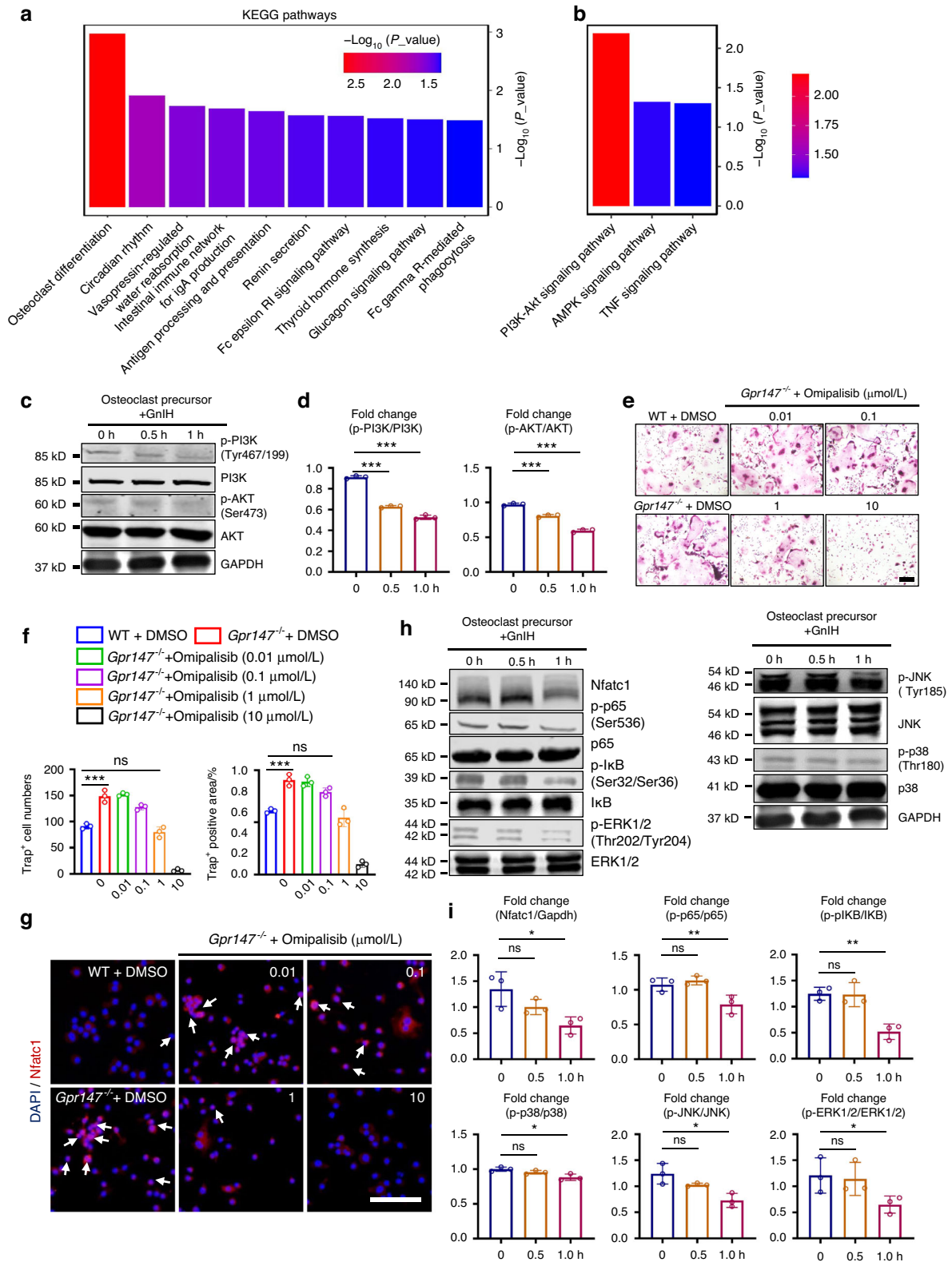


Fig. 4 GnIH/Gpr147 regulates osteoclast function through the PI3K/AKT, MAPK, NF- κ B and Nfatc1 signaling pathway. **a, b** KEGG pathway analysis of the differentiation of WT and *Gpr147*^{-/-} BMMs into osteoclast precursors for 48 h followed by RNA-sequence analysis, $n = 3$ each group. **c, d** The protein levels of PI3K/AKT signaling pathway in WT osteoclast precursors treated with 10 μ mol/L GnIH for the indicated time periods were measured by western blotting. $n = 3$ each group. (*** $P < 0.001$). **e, f** Representative TRAP staining images and quantification of the differentiation of *Gpr147*^{-/-} BMMs into osteoclast cultured with Omipalisib for 5 days. Scale bars: 200 μ m. Trap⁺ cell numbers and area were measured. $n = 3$ each group. (*** $P < 0.001$). **g** Representative Nfatc1 immunofluorescence staining images of osteoclast precursors treated with Omipalisib. $n = 3$ each group. Scale bars: 200 μ m. **h, i** The protein levels of NF- κ B, MAPK and Nfatc1 signaling pathway in WT osteoclast precursors treated with 10 μ mol/L GnIH for the indicated time periods were measured by western blotting. $n = 3$ each group. (* $P < 0.05$, ** $P < 0.01$, *** $P < 0.001$)

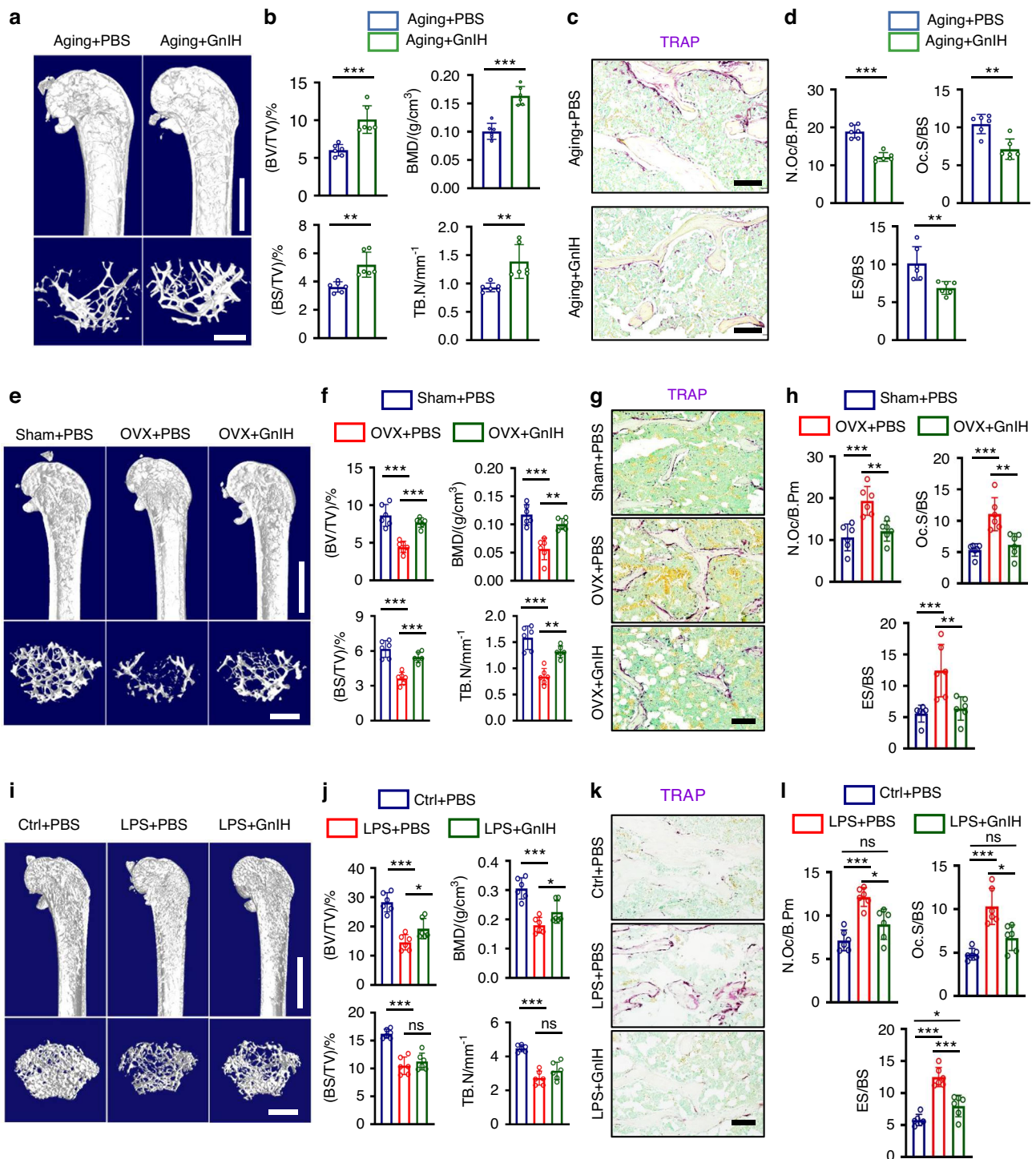


Fig. 5 GnIH prevents aging-, OVX-, and LPS-induced bone loss. **a, b** Representative micro-CT images of femurs (top; scale bars:1 mm) and trabecular bone (bottom; scale bars: 500 μ m) from PBS or 0.1 mg/kg GnIH treatment 18-month-old male mice for 30 days. Quantitation of femur trabecular bone parameters from PBS or 0.1 mg/kg GnIH treatment 18-month-old male mice for 30 days. $n = 6$ each group. (** $P < 0.01$, *** $P < 0.001$). **c, d** Representative TRAP staining images from 0.1 mg/kg GnIH treatment 18-month-old male mice. Scale bars, 100 μ m. The number of N.Oc/B.Pm, Oc.S/BS and ES/BS were quantified. $n = 6$ each group. (** $P < 0.01$, *** $P < 0.001$). **e, f** Representative micro-CT images of femurs (top; scale bars: 1 mm) and trabecular bone (bottom; scale bars: 500 μ m) from Sham, OVX or 0.1 mg/kg GnIH treatment OVX mice for 30 days. Quantitation of femur trabecular bone parameters from Sham, OVX or 0.1 mg/kg GnIH treatment OVX mice for 30 days. $n = 6$ each group. (** $P < 0.01$, *** $P < 0.001$). **g, h** Representative TRAP staining images from 0.1 mg/kg GnIH treatment OVX mice. Scale bars, 100 μ m. The number of N.Oc/B.Pm, Oc.S/BS and ES/BS were quantified. $n = 6$ each group. (** $P < 0.01$, *** $P < 0.001$). **i, j** Representative micro-CT images of femurs (top; scale bars:1 mm) and trabecular bone (bottom; scale bars: 500 μ m) from 0.1 mg/kg GnIH treatment LPS-induced male mice for 7 days. Quantitation of femur trabecular bone parameters from 0.1 mg/kg GnIH treatment LPS-induced male mice for 7 days. $n = 6$ each group. (* $P < 0.05$, *** $P < 0.001$). **k, l** Representative TRAP staining images from 0.1 mg/kg GnIH treatment LPS-induced male mice. Scale bars, 100 μ m. The number of N.Oc/B.Pm, Oc.S/BS and ES/BS were quantified. $n = 6$ each group. (* $P < 0.05$, *** $P < 0.001$)

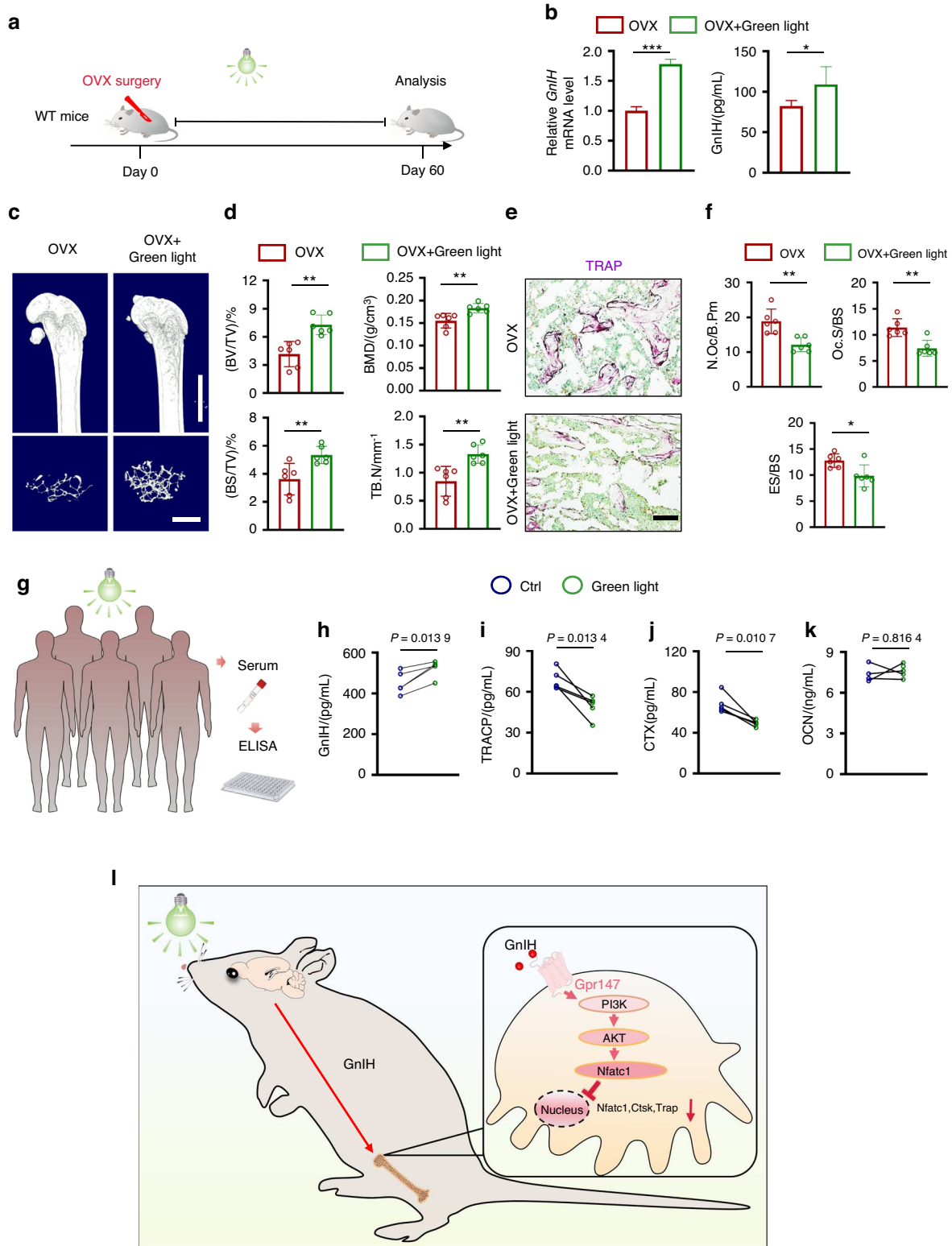


Fig. 6 Green light therapy promotes GnIH release and rescues bone loss in OVX mice. **a** OVX mice were exposed to green (520–525 nm, 400 Lux) light therapy for 8 h (8:00 am–16:00 pm) for 60 days. **b** RT-qPCR analysis of the expression of GnIH in the hypothalamus of OVX mice with or without exposure to green light (left). $n = 3$ each group. Serum GnIH content was detected by ELISA (right). ($*P < 0.05$, $***P < 0.001$). **c, d** Representative micro-CT images of femurs (top; scale bars: 1 mm) and trabecular bone (bottom; scale bars: 500 μm) from OVX mice with or without green light exposure. $n = 6$ each group. ($**P < 0.01$). **e, f** Representative TRAP staining images from OVX mice with or without green light exposure. Scale bars, 100 μm . The number of N.Oc/B.Pm, Oc.S/BS and ES/BS were quantified. $n = 6$ each group. ($*P < 0.05$, $**P < 0.01$). **g** Five subjects were exposed to green (520–525 nm, 400–1000 Lux) light therapy for 2 h (9:00 am–11:00 am) for 7 days. **h–k** Human serum GnIH, bone formation markers (OCN), bone resorption markers (TRACP and CTX) content was detected by ELISA. $n = 5$. Paired t-test. **l** Green light therapy promotes the synthesis and secretion of GnIH in hypothalamus. GnIH is then transported to bone tissue through circulation, binds to osteoclast Gpr147, and inhibits osteoclast differentiation

These results indicate that exposure to green light stimulated the release of GnIH and effectively mitigated bone loss in OVX mice. We conducted further evaluation of the changes in bone mass following green light therapy in *GnIH*^{-/-} and *Gpr147*^{-/-} mice, and the data showed that green light treatment can only partially improve the bone parameters of *GnIH*^{-/-} and *Gpr147*^{-/-} mice (Fig. S11A–E), which may be related to the regulation of melatonin-GnIH pathway by green light.^{36,37}

To examine the prospective utility of green light therapy as a novel clinical approach for treating osteoporosis, we conducted a study involving five healthy adult participants. Each participant underwent a one week of daily green light phototherapy sessions, lasting 2 h per day (Fig. 6g). We evaluated the serum GnIH levels, bone resorption markers and bone formation marker of subjects before and after green light therapy. The results revealed a significant elevation in serum GnIH levels following green light therapy (Fig. 6h). While the serum levels of TRACP and CTX (tartrate acid phosphatase, type I collagen carboxy-terminal peptide, bone resorption markers) were observed to be down-regulated (Fig. 6i, j), and the level of OCN (osteocalcin, bone formation markers) did not change significantly after green light therapy (Fig. 6k). Furthermore, healthy adult participants exposed to regular light showed no significant changes in serum GnIH, OCN, TRACP and CTX (Fig. S12A–D). Our human study was consistent with our animal study and demonstrates the potential of green light therapy in suppressing osteoporosis.

DISCUSSION

The regulatory mechanism that interlinks reproductive hormones and bone homeostasis continues to be an area of ambiguity. For the first time, our study presents groundbreaking evidence demonstrating the involvement of GnIH, a crucial upstream reproductive hormone, in the regulation of bone mass. Our finding revealed that GnIH significantly enhance the function of osteoclasts in vivo and in vitro by inhibiting the receptor Gpr147. In addition, we discovered that both osteoblasts and osteoclasts possess the capability to secrete GnIH, and demonstrated its importance in GnIH/Gpr147 regulation of bone homeostasis. Mechanistically, we demonstrated that GnIH/Gpr147 affects osteoclast differentiation by regulating the PI3K/AKT, MAPK, NF- κ B and Nfat1 signaling pathways. Finally, we found that green light exposure can promote GnIH release and can avoid OVX mice bone loss, and green light therapy significantly downregulated serum levels of bone resorption markers in humans, providing a novel approach for the treatment of osteoporosis disease (Fig. 6l).

Our study further demonstrates that the mechanism of green light therapy in rescuing bone loss in OVX mice probably lies in reducing osteoclast activity through regulating GnIH release, which originates from the hypothalamus and bone tissue. Traditionally, ultraviolet light and infrared light plays a crucial role in bone mass regulation.^{44–46} However, it is important to note that prolonged ultraviolet therapy can cause skin aging and increase the risk of genetic mutations.⁴⁷ Similarly, while far-infrared light may have potential benefits, excessive exposure can damage the skin and eyes.⁴⁸ In comparison, green light is generally considered safer and less harmful to the skin and eyes.⁴⁹ In addition, while green light laser therapy has been shown to promote the differentiation and proliferation of mesenchymal stem cells into osteoblasts, relevant studies have only been conducted at the cellular level, which does not necessarily imply efficacy in vivo. Significantly, our study provides evidence that green light therapy can effectively modulate the levels of bone resorption markers in human serum. This discovery introduces a novel and practical approach that holds promise for the clinical treatment of osteoporosis. However, more detailed investigations into how green light enhances the release of GnIH are needed in the future.

GnRH agonist therapy is commonly utilized in the treatment of certain cancers and individuals with precocious puberty.^{8,50} However, data suggest a potential risk of reduced bone mass following GnRH therapy. As reported, GnIH plays a regulatory role in the synthesis and secretion of GnRH, acting as an inhibitor of GnRH secretion.¹³ It has been reported that GnIH neurons regulate not only GnRH but also Kisspeptin, which is also believed to be a key reproductive hormone upstream of GnRH.^{9,32} Our study has revealed a significant regulatory effect of GnIH on bone mass. Furthermore, our findings may provide an explanation for the association between excessive activation of GnRH and low bone mass. Inadequate synthesis of GnIH may potentially contribute to the increased risk of low bone mass associated with GnRH agonist therapy.

The level of GnIH expression has been linked to abnormal adolescent development and reproductive dysfunction.⁹ The loss of GnIH expression is believed to be a contributing factor to the onset of precocious puberty.³⁴ It is also believed that GnIH antagonists could be developed into drugs for reproductive dysfunction, and whether fertility drugs developed for GnIH/Gpr147 increase the risk of osteoporosis needs to be studied and noted.^{33,51} In our study, we conducted long-term green light therapy on OVX mice, exposing them to up to 8 h per day. It is worth noting that mice are nocturnal animals,⁵² and such prolonged exposure to green light therapy may potentially impact their biological rhythms.⁵³ Therefore, the appropriate duration and intensity of green light illumination in clinical translational therapy require further investigation and discussion. Additionally, the response time to green light therapy may vary among different populations and should be explored further.⁵⁴

In total, our data strongly indicates the role of the key upstream reproductive hormone, GnIH, in regulating bone homeostasis. This study not only advances our understanding of this mechanism but also provides a novel idea and potential method for clinical treatment and prevention of osteoporosis.

MATERIALS AND METHODS

Mouse model

All experimental processes comply with East China Normal University (ECNU) animal ethics (ethical approval number m20230206). ECNU Animal Center provides 8–12 week old or 18 months old WT C57BL/6J mice. It was established that all mice were maintained over a period of 12 h under a complete dark-light cycle (with a white illumination level of 200 lux) as well as a constant temperature and humidity level (20–26 °C), unless otherwise indicated.

GnIH^{-/-} mice and *Gpr147*^{-/-} mice were generated by Cyagen using the CRISPR/Cas9 system in the C57BL/6N mouse strain. To create a GnIH knockout mouse, Exons 1 to 3 were targeted, encompassing a 567 bp coding sequence within the region. Specifically, gRNA1 (GATATTCTATACAGCTAGCTGG) targets exon 1, and gRNA2 (CTTCTCCAGACCTAGTGAACAGG) targets exon 3. For the creation of a Gpr147 knockout mouse, Exons 2 to 3 were targeted, covering a 415 bp coding sequence. Notably, gRNA3 (AGCCCAAGCACTTTCGAAGGTGG) targets exon 2, while gRNA4 (CATGCGACGGAGTAAAGCCAGG) targets exon 3.

Genotype identification of mice was performed using the following primer sequences: *GnIH*^{-/-}-F: CATTTGCCAAATTAGACCT-TAGGG, *GnIH*^{-/-}-R: AAATGCAACCCAGGGTTGATGTC, *GnIH*^{-/-}-He/Wt-F: AGCCCGACTTCAAGAGGCTAC; *Gpr147*^{-/-}-F: GTGGACAGTAAAGTGGGCTTAGGGT, *Gpr147*^{-/-}-R: AGCTAAACAACAGTCTCTGCATG, *Gpr147*^{-/-}-He/Wt-F: GTAATTCTGGGACTGGCACGC.

Cell culture and osteoclast differentiation

Refer to our previous research reports,^{6,55,56} bone marrow macrophages (BMMs) were obtained from the femurs and tibias of 8-week-old WT, *GnIH*^{-/-} or *Gpr147*^{-/-} mouse. They were then cultured in α -MEM medium (Gibco) with the addition of 10 ng/mL M-CSF (R&D), 10% FBS (Gibco), and 1% penicillin-streptomycin

(HyClone). For osteoclast differentiation assay, BMMs were plated in 96-well plates at a density of 1×10^4 cells per well. Subsequently, they were stimulated with 50 ng/mL of RANKL (R&D) and 10 ng/mL of M-CSF (R&D). After 5–7 days, The TRAP staining kit (Sigma-Aldrich) was used to identify TRAP⁺ osteoclasts (five or more nuclei) from osteoclasts fixed in 4% Paraformaldehyde (PFA). For LPS-induced osteoclast differentiation assay, BMMs were plated in 96-well plates at a density of 1×10^4 cells per well. The cells were incubated with 50 ng/mL of RANKL (R&D), 10 ng/mL of M-CSF (R&D), 50 ng/mL of LPS (Beyotime) and 10 μ mol/L GnIH for 5 days. After fixed in 4% PFA, the cells were stained for TRAP assay.^{57–59}

Osteoblast-Osteoclast co-culture

Isolated preosteoblastic cells from the calvaria of 3–5-day-old neonatal mice. Co-culturing was carried out in 96-well plates with BMMs (1×10^4 cells per well) and preosteoblastic cells (1.5×10^3 cells per well) in α -MEM (Gibco) (10% FBS), 100 ng/mL 1 α , 25-dihydropyrene (HyClone), 1% penicillin-streptomycin. One week later, TRAP staining was performed, and the number of osteoclasts exhibiting 5 or more nuclei and positive for TRAP staining was quantified.

CCK-8 assay

After seeding 96-wells with a combination of 100 μ L α -MEM and 20 ng/mL M-CSF-containing BMMs (1.2×10^4 cells per well) for two days, then supplemented with CCK-8 solution (10 μ L per well) for 90 min and read the absorbance at 450 nm.

Cell migration assay

For BMM migration, GnIH at dosages of 0, 0.01, 0.1, 1, 10 μ mol/L was added in the lower chamber while BMMs were seeded in the upper chamber (1×10^5 cells per well) of transwell inserts. After one day, the migrated BMMs were fixed in 4% PFA for 0.5 h, then used water wash 4 times and stained them for 2 h with 0.1% crystal violet. In total, four fields of view were photographed per insert and then quantified using Media Cybernetics' Image-Pro Plus 6.0 (Media Cybernetics).

Treatment with GnIH peptide in vivo

OVX-induced and LPS-induced (LPS was injected intraperitoneally at a dose of 5 mg/kg body weight on day 0 and day 4) bone loss mouse models were used as previously described.^{5,6,60} Mouse GnIH peptide with the sequence Phe-Pro-Ser-Leu-Pro-Gln-Arg-Phe-NH₂ was intraperitoneally injected daily,⁶¹ at the dosage of 0.1 mg/kg in 200 μ L PBS.^{62,63} OVX mice and aging mice were treated with GnIH for one month, LPS-induced mice were treated with GnIH for seven days. GnIH peptide was synthesized by Shanghai Bootech BioScience & Technology.

Green light exposure

The green LED light source (Shanghai wence) was fixed on the top of a special customized cabinet. OVX mice were subjected to green LED light exposure within a custom-designed cabinet, while being provided unrestricted access to food and water. Green light (520–525 nm, 400 Lux) therapy exposure for 8 h (8:00 am–16:00 pm) daily for 60 consecutive days^{38,64} was applied to treated mice. Following daily green light therapy, the mice were subsequently returned to their standard animal housing facility.

A total of five healthy adult males between the ages of 20 and 40, who do not have any visual impairment or eye diseases, have not taken any hormonal or osteoporosis medications within the past three months, and do not have a history of chronic diseases or other medical conditions, were selected for this study. For human green light or regular light exposure experiment, the subjects were initially exposed to regular light for 7 days as control, followed by green light for another 7 days after a two-week rest period. LED green light source emitting wavelengths between 520–525 nm or

regular light (6000 K LED light) were utilized. The experiment took place in their designated room from 9:00 am to 11:00 am daily. The LED green light or regular light source was positioned at a distance of 1–2 m from the subjects' eyes, and the light intensity ranged from 400 to 1 000 lux. To ensure individual comfort, subjects had the flexibility to adjust the distance between the light source and their eyes within the specified range. During the experiment sessions, subjects were specifically instructed to remain awake and maintain a normal blink rate without directly staring at the light source. When exposed to green light or regular light, each subject wore a hospital gown made of the same material. They were encouraged to engage in activities that did not require additional sources of light including conversation and listening to music, while watching television or using screen devices, were forbidden. Subjects were collected for peripheral venous blood sampling before the experiment and after one week of green light or regular light therapy. The experiment underwent thorough review and was approved by the Medical Ethics Committee of Yangzhi Rehabilitation Hospital (Approval No. YZ 2023-070).

Human peripheral blood mononuclear cells differentiation

Obtaining blood from healthy adult individuals. After ficoll centrifugation, human PBMCs were selected and were plated in 96-well plates at a density of 1.5×10^4 cells per well. Subsequently, they were stimulated with 60 ng/mL of RANKL (R&D) and 20 ng/mL of M-CSF (R&D), while treated with the 10 μ mol/L human GnIH with the sequence Val-Pro-Asn-Leu-Pro-Gln-Arg-Phe-NH₂. After 7 days, The TRAP staining kit (Sigma-Aldrich) was used to identify TRAP⁺ osteoclasts (five or more nuclei) from osteoclasts fixed in 4% Paraformaldehyde (PFA). Human GnIH peptide was synthesized by Shanghai Bootech BioScience & Technology.

Western blotting analysis

Following the treatment of cells with GnIH (10 μ mol/L), proceed to lyse the cells using RIPA buffer in order to extract proteins. The protein concentration can then be quantified using the BCA assay (Thermo). Electrophoresis and transfer to nitrocellulose filter membranes (Beyotime) were followed by 3 h of treatment with 5% bovine serum albumin (Beyotime), and incubated with specific antibodies: GAPDH antibody (CST), p-PI3K (Tyr467/199) antibody (Abmart), p-AKT (Ser473) antibody (Abmart), p-p65 (Ser536) antibody (Abmart), p-I κ B (Ser32/Ser36) antibody (Abmart), p-p38 (Thr180) antibody (Abmart), p-JNK (Tyr185) antibody (Abmart), p-ERK (Thr202/Tyr204) antibody (Abmart), p65 antibody (Abmart), I κ B antibody (Abmart), p38 antibody (Abmart), JNK antibody (Abmart), ERK antibody (Abmart), AKT antibody (CST), PI3K antibody (CST), Nfatc1 antibody (SANTA CRUZ). A secondary antibody (Licor) was added to the membranes after overnight incubation at 4 °C. Images were captured using the Odyssey Infrared Imaging System. Image-Pro Plus 6.0 software was used to quantify the bands. First, all readings were normalized to the corresponding band of GAPDH. Next, to calculate the fold changes, p-AKT was normalized to AKT samples, p-PI3K was normalized to PI3K samples, p-p65 was normalized to p65 samples, p-I κ B was normalized to I κ B samples, p-p38 was normalized to p38 samples, p-JNK was normalized to JNK samples and p-ERK was normalized to ERK samples.

Immunofluorescence staining

For paraffin sections, after treatment with gradient of dehydration and 20 mg/mL proteinase K for 20 min, paraffin sections were fixed in 2% BSA and 0.1% Triton X-100 buffers for 1 h, they were incubated overnight at 4 °C with first antibody Trap (Novus), then with secondary antibody for 1 h, followed by DAPI staining for nuclei (Sigma).⁶⁵

RNA and RT-qPCR

RNA and cDNA were extracted separately using Trizol (Invitrogen, USA) and 2 \times Hifair® II. SuperMix (Yeasen, China). Subsequently, the

quantitative real-time PCR (RT-qPCR) reaction was performed using the Hieff® qPCR SYBR® Green Master Mix (YEASEN). Hypothalamic tissue was isolated from the brains of mice treated with green light, and the bone tissue was derived from the femur of the mouse after stripping the muscle tissue. The tissues were snap-frozen using liquid nitrogen and subsequently pulverized. BMMs and BMSC were isolated from 8-week-old WT mice. Osteoblasts and chondrocytes were differentiated from BMSCs, while osteoclasts were differentiated from BMMs.

The PCR primer sequences are as follows: Nfatc1-F: CCCGTCA-CATTCTGGTCCAT, Nfatc1-R: CAAGTAACCGTGTAGCTGCACAA; Ctsk-F: ATGTGGGTGTTCAAGTTTCTGC, Ctsk-R: CCACAAGATTCTGGG-GACTC; Trap-F: CAGCTCCCTAGAAGA TGGATTAT, Trap-R: GTCAG-GAGTGGGAGCCATATG; Actin-F: GTACGCCAACACAGTGCTG, Actin-R: CGTCATACTCTGCTTGCTG; GnIH-F: CAAGACACCCGCTGATTTGC, GnIH-R: TTCGCTTCCACCAGGACTC; Gpr147-F: CCGAGTCTGAACGA-GAGTGA, Gpr147-R: CGGTCTTAAGCAGATGAA;

RNA-sequencing analysis

BMMs were isolated from 8-week-old WT and *Gpr147*^{-/-} mouse and then stimulated with RANKL (50 ng/mL) and M-CSF (10 ng/mL) for 48 h. Cells were lysed using Trozil and sent to Shanghai Origin-gene Biological Company for RNA extraction, sequencing and analysis. Genes exhibiting a false discovery rate (FDR) < 0.05 were classified as differentially expressed.

Micro-CT

Femurs of mice were fixed in 4% PFA for 48 h and washed with water 4 times, then transferred into 75% alcohol for preservation. Skyscan-1272 micro-CT (Bruker micro-CT, Belgium) was used to examine the bone micro-architecture related parameters including bone mineral density (BMD), bone volume density (BV/TV), bone area density (BS/TV), trabecular number (Tb.N) and trabecular thickness (Tb.Th). The following software was used: Skyscan NRecon software (Bruker), CT Analyser software (Bruker), CT Voxsoftware (Bruker), and scanning parameters and analysis methods were as previously described.^{6,7}

TRAP staining

After treatment with a dehydration gradient, the paraffin sections were treated with 0.1% Triton X-100 for 30 min and washed with PBS 2 times, and then stained with TRAP staining kit (Sigma-Aldrich) at 37°C for 1 h. The OsteoMeasure Analysis System (Osteometrics) was used to analyze the number, surface area and eroded surface area of osteoclast. For calvarias TRAP staining, calvarias were isolated and fixed in 4% PFA for 24 h, then treated with 0.1% Triton X-100 for 1 h and washed with PBS 5 times. After stained with TRAP staining kit at 37°C for 4 h, the positive area were determined using the Image-Pro Plus 6.0 software.

Calcein labeling

WT, *GnIH*^{-/-} and *Gpr147*^{-/-} mice were injected with calcein (30 mg/kg) on postnatal day 55 and postnatal day 65, and euthanized on postnatal day 72. Vertebrae were fixed in 4% PFA for 24 h, processed through an alcohol dehydration gradient, then embedded with methyl methacrylate. 5 µm sections were cut for calcein double labeling analysis and Goldner's staining. For Goldner's staining, the sections were stained with hematoxylin, Ponceau Acid, Orange G and light green solution. The OsteoMeasure Analysis System (Osteometrics) were used to measure bone formation rate per bone surface, mineral apposition rate, osteoblast number, osteoblast surface area, and osteoids per bone surface.

Elisa assay

Analysis of GnIH levels in mouse serum by using the KL-GnIH-Mu kit (Kanglang). Analysis of TNF-α, IL-1β, IL-6 levels in mouse serum by using the ELISA Kit (Jingmei). Analysis of GnIH, TRACP, CTX, OCN levels in human serum by using the ELISA Kit (Jingmei).

Statistical analysis

All data are reported as means ± SD. GraphPad Prism 8.0 was employed to evaluate significant differences in the data. One-way ANOVA followed by Tukey's *t* tests or two-way ANOVA followed by Tukey's *t* tests was used for multiple comparisons. When comparing only two groups, paired or unpaired Student's *t* test was used as appropriate. Statistical significance was *P* < 0.05.

AUTHOR CONTRIBUTIONS

The experimental design and research supervision were carried out by Jian Luo and Mingyao Liu. Yu You, Konglin Huo, Liang He, Tongyue Wang, Lei Zhao, Rong Li, Xiaoqing Chen, Xuebin Ma, Zhiying Yue performed experiments. Lujian Liao, Ning Wang and Stefan Sivko analyzed and interpreted data. Jian Luo, Yu You and Ning Wang wrote or edited the manuscript. All authors approved the final version.

FUNDING

This work is supported by grants from the National Key Research and Development Program of China (2023YFB3810200 to J.L.), the National Natural Science Foundation of China (92168204, 82225030 to J.L.), and the Fundamental Research Funds for the Central Universities (22120210586 to J.L.).

ADDITIONAL INFORMATION

Supplementary information The online version contains supplementary material available at <https://doi.org/10.1038/s41413-024-00389-7>.

Competing interests: The authors declare no competing interests.

REFERENCES

1. Feng, X. & McDonald, J. M. Disorders of bone remodeling. *Annu. Rev. Pathol.* **6**, 121–145 (2011).
2. Yamaguchi, M. Role of carotenoid β-cryptoxanthin in bone homeostasis. *J. Biomed. Sci.* **19**, 36 (2012).
3. Zhu, Q. et al. OTUB1 promotes osteoblastic bone formation through stabilizing FGFR2. *Signal Transduct. Target Ther.* **8**, 142 (2023).
4. Li, C. et al. The osteoprotective role of USP26 in coordinating bone formation and resorption. *Cell Death Differ.* **29**, 1123–1136 (2022).
5. Li, Z. et al. Dual targeting of bile acid receptor-1 (TGR5) and farnesoid X receptor (FXR) prevents estrogen-dependent bone loss in mice. *J. Bone Miner. Res.* **34**, 765–776 (2019).
6. Luo, J. et al. LGR4 is a receptor for RANKL and negatively regulates osteoclast differentiation and bone resorption. *Nat. Med.* **22**, 539–546 (2016).
7. Sun, P. et al. Regulation of body length and bone mass by *Gpr126/Adgrg6*. *Sci. Adv.* **6**, eaaz0368 (2020).
8. Mills, E. G. et al. The relationship between bone and reproductive hormones beyond estrogens and androgens. *Endocr. Rev.* **42**, 691–719 (2021).
9. Tsutsui, K. & Ubuka, T. Gonadotropin-inhibitory hormone (GnIH): a new key neurohormone controlling reproductive physiology and behavior. *Front. Neuroendocrinol.* **61**, 100900 (2021).
10. Yeh, J. K., Chen, M. M. & Aloia, J. F. Ovariectomy-induced high turnover in cortical bone is dependent on pituitary hormone in rats. *Bone* **18**, 443–450 (1996).
11. Yeh, J. K., Chen, M. M. & Aloia, J. F. Effects of 17 beta-estradiol administration on cortical and cancellous bone of ovariectomized rats with and without hypophysectomy. *Bone* **20**, 413–420 (1997).
12. Wu, X. Y. et al. Early bone mineral density decrease is associated with FSH and LH, not estrogen. *Clin. Chim. Acta* **415**, 69–73 (2013).
13. Maggi, R. et al. GnRH and GnRH receptors in the pathophysiology of the human female reproductive system. *Hum. Reprod. Update* **22**, 358–381 (2016).
14. Brommage, R. et al. High-throughput screening of mouse gene knockouts identifies established and novel skeletal phenotypes. *Bone Res.* **2**, 14034 (2014).
15. Jiang, C., Qi, L., Xue, J. & Wang, Y. Indirubin-3'-oxime promotes the efficacy of GnRHα in obese-induced central precocious puberty and maintains normal bone growth and body weight via the ERK-Sp1-KISS-1/GPR54 axis. *Cell Mol. Biol.* **69**, 188–194 (2023).
16. Allan, C. M. et al. Follicle-stimulating hormone increases bone mass in female mice. *Proc. Natl. Acad. Sci. USA* **107**, 22629–22634 (2010).
17. Divasta, A. D., Laufer, M. R. & Gordon, C. M. Bone density in adolescents treated with a GnRH agonist and add-back therapy for endometriosis. *J. Pediatr. Adolesc. Gynecol.* **20**, 293–297 (2007).

18. Rothman, M. S. & Wierman, M. E. The role of gonadotropin releasing hormone in normal and pathologic endocrine processes. *Curr. Opin. Endocrinol. Diab. Obes.* **14**, 306–310 (2007).
19. Sauerbrun-Cutler, M. T. & Alvero, R. Short- and long-term impact of gonadotropin-releasing hormone analogue treatment on bone loss and fracture. *Fertil. Steril.* **112**, 799–803 (2019).
20. Sun, L. et al. FSH directly regulates bone mass. *Cell* **125**, 247–260 (2006).
21. Talbi, R. & Navarro, V. M. Novel insights into the metabolic action of Kiss1 neurons. *Endocr. Connect* **9**, R124–R133 (2020).
22. Celik, O. et al. Ghrelin action on GnRH neurons and pituitary gonadotropes might be mediated by GnIH-GPR147 system. *Horm. Mol. Biol. Clin. Investig.* **25**, 121–128 (2016).
23. Singh, P., Anjum, S., Srivastava, R. K., Tsutsui, K. & Krishna, A. Central and peripheral neuropeptide RFRP-3: A bridge linking reproduction, nutrition, and stress response. *Front. Neuroendocrinol.* **65**, 100979 (2022).
24. Tsutsui, K., Ubuka, T., Bentley, G. E. & Kriegsfeld, L. J. Gonadotropin-inhibitory hormone (GnIH): discovery, progress and prospect. *Gen. Comp. Endocrinol.* **177**, 305–314 (2012).
25. Ubuka, T., Bentley, G. E., Ukena, K., Wingfield, J. C. & Tsutsui, K. Melatonin induces the expression of gonadotropin-inhibitory hormone in the avian brain. *Proc. Natl. Acad. Sci. USA* **102**, 3052–3057 (2005).
26. Luo, R. et al. Possible role of GnIH as a novel link between hyperphagia-induced obesity-related metabolic derangements and hypogonadism in male mice. *Int. J. Mol. Sci.* **23**, 8066 (2022).
27. Tsutsui, K. et al. Gonadotropin-inhibitory hormone (GnIH) and its control of central and peripheral reproductive function. *Front. Neuroendocrinol.* **31**, 284–295 (2010).
28. Tsutsui, K. & Ubuka, T. GnIH control of feeding and reproductive behaviors. *Front. Endocrinol.* **7**, 170 (2016).
29. Tsutsui, K., Ubuka, T. & Ukena, K. Advancing reproductive neuroendocrinology through research on the regulation of GnIH and on its diverse actions on reproductive physiology and behavior. *Front. Neuroendocrinol.* **64**, 100955 (2022).
30. Gojska, N. M. & Belsham, D. D. Glucocorticoid receptor-mediated regulation of Rfrp (GnIH) and Gpr147 (GnIH-R) synthesis in immortalized hypothalamic neurons. *Mol. Cell Endocrinol.* **384**, 23–31 (2014).
31. Poling, M. C. & Kauffman, A. S. Regulation and function of RFRP-3 (GnIH) neurons during postnatal development. *Front. Endocrinol.* **6**, 150 (2015).
32. Tsutsui, K. A new key neurohormone controlling reproduction, gonadotropin-inhibitory hormone (GnIH): Biosynthesis, mode of action and functional significance. *Prog. Neurobiol.* **88**, 76–88 (2009).
33. Tsutsui, K. & Ubuka, T. Discovery of gonadotropin-inhibitory hormone (GnIH), progress in GnIH research on reproductive physiology and behavior and perspective of GnIH research on neuroendocrine regulation of reproduction. *Mol. Cell Endocrinol.* **514**, 110914 (2020).
34. Ubuka, T., Son, Y. L., Tobar, Y. & Tsutsui, K. Gonadotropin-inhibitory hormone action in the brain and pituitary. *Front. Endocrinol.* **3**, 148 (2012).
35. Mittan, D. et al. Bone loss following hypogonadism in men with prostate cancer treated with GnRH analogs. *J. Clin. Endocrinol. Metab.* **87**, 3656–3661 (2002).
36. Zhang, L. et al. Green light inhibits GnRH-I expression by stimulating the melatonin-GnIH pathway in the chick brain. *J. Neuroendocrinol.* **29**, 1–15 (2017).
37. Zhu, H. X. et al. Effect and molecular regulatory mechanism of monochromatic light colors on the egg-laying performance of Yangzhou geese. *Anim. Reprod. Sci.* **204**, 131–139 (2019).
38. Tang, Y. L. et al. Green light analgesia in mice is mediated by visual activation of enkephalinergic neurons in the ventrolateral geniculate nucleus. *Sci. Transl. Med.* **14**, eabq6474 (2022).
39. Cui, J. et al. Triptolide prevents bone loss via suppressing osteoclastogenesis through inhibiting PI3K-AKT-NFATc1 pathway. *J. Cell Mol. Med.* **24**, 6149–6161 (2020).
40. Qian, Z. et al. Cytisine attenuates bone loss of ovariectomy mouse by preventing RANKL-induced osteoclastogenesis. *J. Cell Mol. Med.* **24**, 10112–10127 (2020).
41. Xin, Y. et al. New Function of RUNX2 in Regulating Osteoclast Differentiation via the AKT/NFATc1/CTSK Axis. *Calcif. Tissue Int.* **106**, 553–566 (2020).
42. Yang, S. et al. AKT/GSK3 β /NFATc1 and ROS signal axes are involved in AZD1390-mediated inhibitory effects on osteoclast and OVX-induced osteoporosis. *Int. Immunopharmacol.* **113**, 109370 (2022).
43. Kovtonyuk, L. V. et al. IL-1 mediates microbiome-induced inflammation of hematopoietic stem cells in mice. *Blood* **139**, 44–58 (2022).
44. Cui, J., Fu, Y., Yi, Z., Dong, C. & Liu, H. The beneficial effects of ultraviolet light supplementation on bone density are associated with the intestinal flora in rats. *Appl. Microbiol. Biotechnol.* **105**, 3705–3715 (2021).
45. Kimlin, M. G. Geographic location and vitamin D synthesis. *Mol. Asp. Med.* **29**, 453–461 (2008).
46. Lu, Y., Yang, J., Dong, C., Fu, Y. & Liu, H. Gut microbiome-mediated changes in bone metabolism upon infrared light exposure in rats. *J. Photochem. Photobiol. B* **217**, 112156 (2021).
47. Narayanan, D. L., Saladi, R. N. & Fox, J. L. Ultraviolet radiation and skin cancer. *Int. J. Dermatol.* **49**, 978–986 (2010).
48. Bergamaschi, A., Grandi, C., D'Addato, M., Di Carlo, V. & Russo, A. Health risks from infrared emissions from radiant tube heaters in the workplace]. *G Ital. Med. Lav.* **17**, 41–49 (1995).
49. Christensen, T., Kinn, G., Granli, T. & Amundsen, I. Cells, bilirubin and light: formation of bilirubin photoproducts and cellular damage at defined wavelengths. *Acta Paediatr.* **83**, 7–12 (1994).
50. Rachner, T. D., Coleman, R., Hadji, P. & Hofbauer, L. C. Bone health during endocrine therapy for cancer. *Lancet Diab. Endocrinol.* **6**, 901–910 (2018).
51. Tsutsui, K., Son, Y. L., Kiyohara, M. & Miyata, I. Discovery of GnIH and its role in hypothyroidism-induced delayed puberty. *Endocrinology* **159**, 62–68 (2018).
52. Jensen, T. L., Kiersgaard, M. K., Sørensen, D. B. & Mikkelsen, L. F. Fasting of mice: a review. *Lab. Anim.* **47**, 225–240 (2013).
53. Wetterberg, L. Light and biological rhythms. *J. Intern. Med.* **235**, 5–19 (1994).
54. Brown, T. M. et al. Recommendations for daytime, evening, and nighttime indoor light exposure to best support physiology, sleep, and wakefulness in healthy adults. *PLoS Biol.* **20**, e3001571 (2022).
55. Jiang, W. et al. PGE2 activates EP4 in subchondral bone osteoclasts to regulate osteoarthritis. *Bone Res.* **10**, 27 (2022).
56. Yue, Z. et al. RSPO2 and RANKL signal through LGR4 to regulate osteoclastic premetastatic niche formation and bone metastasis. *J. Clin. Invest.* **132**, e144579 (2022).
57. Hou, G. Q. et al. Lipopolysaccharide (LPS) promotes osteoclast differentiation and activation by enhancing the MAPK pathway and COX-2 expression in RAW264.7 cells. *Int. J. Mol. Med.* **32**, 503–510 (2013).
58. Mao, J. Y. et al. Serum amyloid A enrichment impairs the anti-inflammatory ability of HDL from diabetic nephropathy patients. *J. Diab. Complications* **31**, 1538–1543 (2017).
59. Zhu, Y., Liu, Z., Peng, Y. P. & Qiu, Y. H. Interleukin-10 inhibits neuroinflammation-mediated apoptosis of ventral mesencephalic neurons via JAK-STAT3 pathway. *Int. Immunopharmacol.* **50**, 353–360 (2017).
60. Sharma, K. et al. Chebulinic acid alleviates LPS-induced inflammatory bone loss by targeting the crosstalk between reactive oxygen species/NF κ B signaling in osteoblast cells. *Free Radic. Biol. Med.* **194**, 99–113 (2023).
61. Constantin, S. et al. An inhibitory circuit from brainstem to GnRH neurons in male mice: a new role for the RFRP Receptor. *Endocrinology* **162**, bqab030 (2021).
62. Huo, K. et al. RFRP-3, the mammalian ortholog of GnIH, is a novel modulator involved in food intake and glucose homeostasis. *Front. Endocrinol.* **11**, 194 (2020).
63. Ullah, R. et al. Gonadotropin inhibitory hormone and RF9 stimulate hypothalamic-pituitary-adrenal axis in adult male rhesus monkeys. *Neuropeptides* **66**, 1–7 (2017).
64. An, K. et al. A circadian rhythm-gated subcortical pathway for nighttime-light-induced depressive-like behaviors in mice. *Nat. Neurosci.* **23**, 869–880 (2020).
65. He, L. et al. GPRCSB protects osteoarthritis by regulation of autophagy signaling. *Acta Pharm. Sin. B* **13**, 2976–2989 (2023).



Open Access This article is licensed under a Creative Commons Attribution 4.0 International License, which permits use, sharing, adaptation, distribution and reproduction in any medium or format, as long as you give appropriate credit to the original author(s) and the source, provide a link to the Creative Commons licence, and indicate if changes were made. The images or other third party material in this article are included in the article's Creative Commons licence, unless indicated otherwise in a credit line to the material. If material is not included in the article's Creative Commons licence and your intended use is not permitted by statutory regulation or exceeds the permitted use, you will need to obtain permission directly from the copyright holder. To view a copy of this licence, visit <http://creativecommons.org/licenses/by/4.0/>.